Measurement of turbulent velocity and bounds for thermal diffusivity in laser shock compressed foams by X-ray photon correlation spectroscopy - Supplementary Information

Charles Heaton,[1,*] Hao Yin,[2,3] Dimitri Khaghani,[4] Hae Ja Lee,[4] Hannah Poole,[1,5] Eric Blackman,[3,5,6] Nina Boiadjieva,[4] Xiaoqian M. Chen,[7] Celine Crépisson,[1] Gilbert W. Collins,[2,5,3,6] Adrien Descamps,[8] Arianna E. Gleason,[4] Cristian Gutt,[9] Alexander N. Petsch,[4,10] Lisa Randolph,[11] Silke Nelson,[4] Peregrine McGehee,[4] Rajan Plumley,[4,10,12] Christopher Spindloe,[13] Thomas Stevens,[1] Charlotte Stuart,[1] Joshua J. Turner,[4,10] Hussein Aluie,[2,3,6] Jessica K. Shang,[2,3,6] and Gianluca Gregori[1]

[1] *Department of Physics, University of Oxford, Parks Road, Oxford OX1 3PU, United Kingdom*
[2] *Department of Mechanical Engineering, University of Rochester, Rochester, NY 14627, USA*
[3] *Center for Matter at Atomic Pressures, University of Rochester, Rochester, NY 14627, USA*
[4] *SLAC National Accelerator Laboratory, 2575 Sand Hill Road, Menlo Park, California 94025, USA*
[5] *Department of Physics and Astronomy, University of Rochester, NY 14627, USA*
[6] *Laboratory for Laser Energetics, University of Rochester, Rochester, NY 14623, USA*
[7] *National Synchrotron Light Source II, Brookhaven National Laboratory, Upton, New York 11973, USA*
[8] *School of Mathematics and Physics, Queens University Belfast, University Road, Belfast BT7 1NN, United Kingdom*
[9] *Department of Physics, University of Siegen, Emmy-Noether-Campus, Walter-Flex-Str. 3, 57072 Siegen, Germany*
[10] *Stanford Institute for Materials and Energy Sciences, Stanford University, Stanford, CA, USA*
[11] *European XFEL, Holzkoppel 4, 22869, Schenefeld, Germany*
[12] *Department of Physics, Carnegie Mellon University, 5000 Forbes Ave, Pittsburgh, PA 15213, USA*
[13] *Central Laser Facility (CLF), STFC Rutherford Appleton Laboratory, Harwell Campus, Didcot OX11 0QX, United Kingdom*

(Dated: September 30, 2025)

SOURCE MONITOR

X-ray photon correlation spectroscopy requires that the probe source is coherent, both in space and time. While XFEL radiation is spatially coherent, SASE radiation is not coherent in time due to the randomly seeded spikes. We therefore utilize LCLS's self seeding operation to ensure temporal coherence. To optimize seeding performance and assess temporal coherence, a transmissive spectrometer based on the design of Zhu et al. (2012) [1] is used. A 10 μm thin cylindrically bent silicon crystal upstream of the target chamber is used to disperse the incoming X-ray beam which is imaged onto a detector. Fig. 1 gives an illustrative example of a spectrum measured when in self-seeding operation.

MODEL FOR $F_{\mathrm{Plasma}}(q,\tau)$

The model we use for fitting $F(q,\tau)$ derives from the work of Mithen et al. (2011) [2] who use a hydrodynamic description to model ion dynamics a strongly coupled plasma. They use the linearized hydrodynamic equations to formulate that

$$\frac{S(q,\omega)}{S(q)} = \frac{\gamma-1}{\gamma}\ \frac{2D_T q^2}{\omega^2+\left(D_T q^2\right)^2} + \frac{1}{\gamma}\left(\frac{\sigma q^2}{\left(\omega+c_s q\right)^2+\left(\sigma q^2\right)^2} + \frac{\sigma q^2}{\left(\omega-c_s q\right)^2+\left(\sigma q^2\right)^2}\right) \tag{1}$$

* charles.heaton@physics.ox.ac.uk

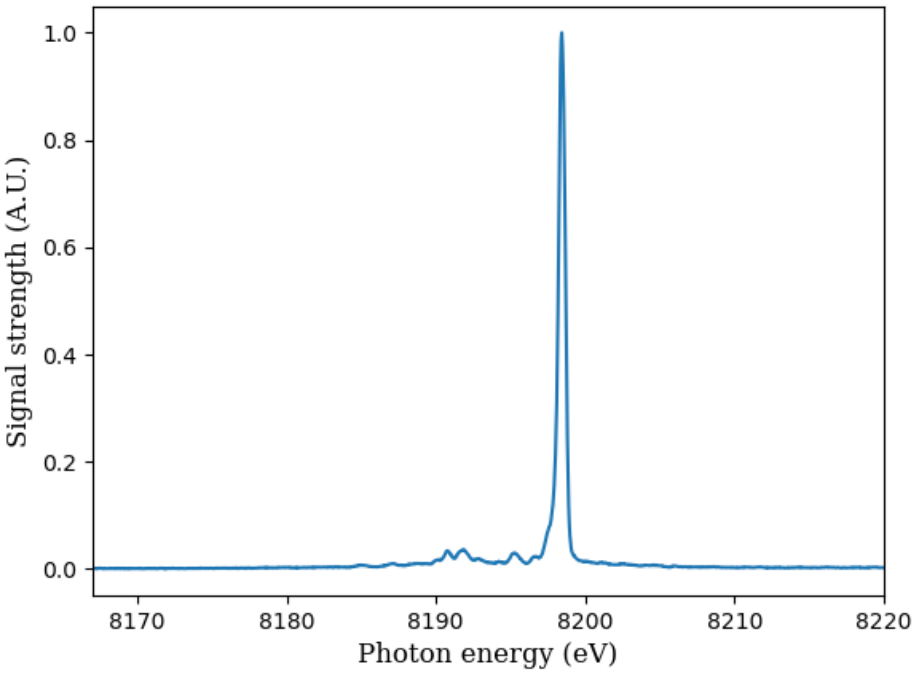

Figure 1: Source spectrum measured while in self seeded mode.

where γ is the adiabatic index of the plasma, D_T is the thermal diffusivity, c_s is the adiabatic sound speed and σ is the sound attenuation coefficient. To find the equivalent $F_{\text{Plasma}}(q,\tau)$ an inverse Fourier transform needs to be performed. Lorentzian pulses are transformed under an inverse Fourier transform to exponential complex exponential decays

$$\mathcal{F}^{-1}\left(\frac{2a}{(b+\omega)^2+a^2}\right) = \exp\left(-a\left|t\right| - ibt\right). \tag{2}$$

Therefore, $F(q,\tau)$, normalised to the static structure factor, is

$$\begin{aligned} F_{\text{Plasma}}(q,\tau) &= \frac{\gamma-1}{\gamma}\exp\left(-D_T q^2\tau\right) + \frac{1}{2\gamma}\left(\exp\left(-\sigma q^2\tau\right)\left(\exp\left(-ic_s q\tau\right) + \exp\left(ic_s q\tau\right)\right)\right) \\ &= \frac{\gamma-1}{\gamma}\exp\left(-D_T q^2\tau\right) + \frac{1}{\gamma}\left(\exp\left(-\sigma q^2\tau\right)\cos\left(c_s q\tau\right)\right). \end{aligned} \tag{3}$$

The acoustic term $\cos\left(c_s q\tau\right)$ is expected to vary on much faster timescales than the nanosecond probe timescale, on the order of a few ps. Therefore, the second term will oscillate very rapidly between -1 and 1. Over the probed timescales therefore, we argue that this term will average to zero. We therefore have

$$F_{\text{Plasma}}(q,\tau) = \frac{\gamma-1}{\gamma}\exp\left(-D_T q^2\tau\right). \tag{4}$$

This approximation for $F(q,\tau)$ does not obey the condition that $F_{\text{Plasma}}(q,0) = 1$ and so therefore, we make the approximation that $\gamma >> 1$ to enforce the property that $\lim_{\tau\to 0} F(q,\tau) = 1$.

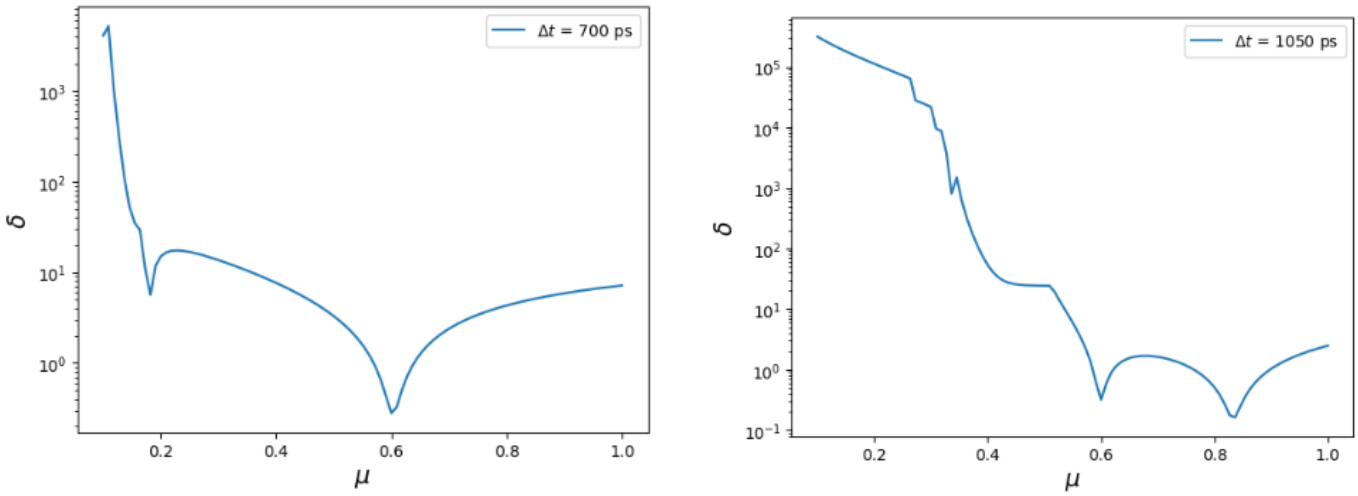

Figure 2: Fitting procedure for $\Delta t = 700$ ps and $\Delta t = 1050$ ps shots. The fitted μ for $\Delta t = 700$ ps, **left**, is found to be 0.60 and 0.84 for $\Delta t = 1050$ ps, **right**, operation modes.

FITTING FOR SPATIAL OVERLAP

Unfortunately, it was not possible to quantify the degree of spatial overlap μ on the beamtime. We therefore need to infer this from the XSVS data. As outlined in the paper, we do this by fitting the XSVS data to the full intermediate scattering function

$$|F(q,\tau)|^2 = \exp\left(-\frac{v_0\tau}{L}\right)\exp\left(-2q^2D_T\tau\right)\exp\left(-\left(\delta v\ q\ \tau\right)^2\right). \tag{5}$$

μ, along with the pulse intensity ratio and β_0, will determine the "working distance" - how much a change in $|F(q,\tau)|^2$ decreases the measured contrast. Therefore, changing μ will change the calculated $|F(q,\tau)|^2$. In particular, we monitor the error in the calculated v_0 as we have a calculated particle velocity from VISAR, which determines $|F(0,\tau)|^2$. To define a spatial overlap, we calculate $|F(q,\tau)|^2$ for a set of μ and record the figure of merit, δ, defined by

$$\delta = \sqrt{\left(\frac{v_0^{(\mathrm{fit})} - v_0^{(\mathrm{VISAR})}}{\sigma_{v_0}^{(\mathrm{VISAR})}}\right)^2 + \left(\frac{\sigma_{v_0}^{(\mathrm{fit})}}{v_0^{(\mathrm{fit})}}\right)^2} \tag{6}$$

where $v_0^{(\mathrm{fit})}$ is the fitted particle velocity, $v_0^{(\mathrm{VISAR})}$ is the VISAR (and equation of state) inferred particle velocity, $\sigma_{v_0}^{(\mathrm{VISAR})}$ is the error on the VISAR inferred velocity and $\sigma_{v_0}^{(\mathrm{fit})}$ is the error on the fitted velocity. Fig. 2 demonstrates this procedure for the two shots included in the thermal diffusivity calculation.

DERIVATION OF INTENSITY DISTRIBUTION OF A SPECKLE PATTERN

X-ray speckle visibility spectroscopy (XSVS) requires an accurate method to extract the contrast of a speckle pattern. A rigorous treatment of the statistical properties of speckle patterns can be found in Goodman (1975) [3] where it is argued that for a perfectly coherent speckle, $\beta = 1$, the intensity distribution should follow an exponential distribution

$$P_i(I) = \frac{1}{2\sigma_i^2}\exp\left(-\frac{I}{2\sigma_i^2}\right). \tag{7}$$

If the probe volume is larger than the coherence volume, $\frac{V_{\text{probe}}}{V_{\text{coh}}} = N > 1$, the detector records N independent speckle patterns $I = \sum_i^N I_i$. Goodman argues that the resulting intensity distribution can be found by considering the Fourier transform of the distribution

$$M_i(\omega) = \mathcal{F}[P_i(I)](\omega) = \frac{1}{1 - i\omega\overline{I_i}} \tag{8}$$

where $\overline{I_i}$ is the mean intensity of the i^{th} speckle pattern. The Fourier transform of N independent speckle distributions will be the product of all $M_i(\omega)$

$$M_N(\omega) = \prod_i^N M_i(\omega) = \prod_i^N \frac{1}{1 - i\omega\overline{I_i}}. \tag{9}$$

If one assumes that the contribution from each speckle pattern is equal, $\overline{I} = I_0$, the inverse Fourier transform recovers the Γ distribution. Photon statistics in a speckle pattern should follow the Γ distribution.

DISCRETE Γ DISTRIBUTION AND ITS MOMENTS

Ordinarily when analyzing speckle data, a Γ distribution is fitted to the data to infer a contrast [3]. The Γ distribution is defined as

$$P_\Gamma(k \mid \overline{k}, \beta) = \frac{\frac{1}{\beta}^{\frac{1}{\beta}} \left(\frac{k}{\overline{k}}\right)^{\frac{1}{\beta}-1} \exp\left(-\frac{k}{\overline{k}\beta}\right)}{\Gamma(\beta^{-1})}. \tag{10}$$

This can be simplified if the following substitutions are made $M = \frac{1}{\beta}$ and $\theta = \overline{k}\beta$

$$P_\Gamma(k|\ M, \theta) = \frac{\theta^{-M} k^{M-1} \exp\left(-\frac{k}{\theta}\right)}{\Gamma(M)}. \tag{11}$$

Moments, $E(K)$ and $E(K^2)$, can be found to show that $\frac{\text{Var(k)}}{\mu(k)^2} = \beta$ as argued in the paper. The first moment is defined as

$$\begin{aligned} E(k) &= \int_0^\infty k \frac{\theta^{-M} k^{M-1} \exp\left(-\frac{k}{\theta}\right)}{\Gamma(M)} \mathrm{d}k \\ &= \frac{\theta^{-M}}{\Gamma(M)} \int_0^\infty k^M \exp\left(-\frac{k}{\theta}\right) \mathrm{d}k \\ &= \frac{\theta^{-M}}{\Gamma(M)} \left[-\theta^{M+1}\ \gamma\left(M+1, \frac{k}{\theta}\right)\right]_0^\infty \end{aligned} \tag{12}$$

where γ is the incomplete Γ function which is defined as

$$\gamma(a, b) = \int_b^\infty t^{a-1} e^{-t} \mathrm{d}t. \tag{13}$$

$\gamma(a, b)$ has the properties

$$\gamma(a, 0) = \int_0^\infty t^{a-1} e^{-t} \mathrm{d}t = \Gamma(a) \tag{14}$$

and

$$\lim_{b\to\infty}\gamma(a,b)=0. \tag{15}$$

Therefore,

$$\begin{aligned} E(K) &= \frac{\theta^{-M}\theta^{M+1}}{\Gamma(M)}\left[(0)-(-\Gamma(M+1))\right] \\ &= \theta M = \overline{k} \end{aligned} \tag{16}$$

as expected. $E(K^2)$ is defined similarly as

$$\begin{aligned} E(K^2) &= \int_0^\infty k^2 \frac{\theta^{-M}k^{M-1}\exp\left(-\frac{k}{\theta}\right)}{\Gamma(M)}\mathrm{d}k \\ &= \frac{\theta^{-M}}{\Gamma(M)}\int_0^\infty k^{M+1}\exp\left(-\frac{k}{\theta}\right)\mathrm{d}k \\ &= \frac{\theta^{-M}}{\Gamma(M)}\left[-\theta^{M+2}\,\gamma\left(M+2,\frac{k}{\theta}\right)\right]_0^\infty . \end{aligned} \tag{17}$$

Following the same logic as before, one recovers

$$\begin{aligned} E(K^2) &= \frac{\theta^{-M}\theta^{M+2}}{\Gamma(M)}\left[(0)-(-\Gamma(M+2))\right] \\ &= \theta^2\frac{\Gamma(M+2)}{\Gamma(M)} \\ &= \theta^2\frac{(M+1)(M)\Gamma(M)}{\Gamma(M)} \\ &= \theta^2\ (M+1)(M) \\ &= \beta^2\overline{k}^2\ \frac{1}{\beta}\ \left(1+\frac{1}{\beta}\right) \\ &= \overline{k}^2\beta\ \frac{\beta+1}{\beta} = \overline{k}^2\left(\beta+1\right). \end{aligned} \tag{18}$$

Given $\mathrm{Var}(k)=E(K^2)-E(K)^2$,

$$\mathrm{Var}(k)=\overline{k}^2(\beta+1)-\overline{k}^2=\overline{k}^2\beta. \tag{19}$$

We therefore have Var(k) $/E(K)^2=\beta$ as is required.

However, in our experiment we are neither in the sparse photon limit, where single photon counting statistics necessitate the use of the Poisson-Γ distribution [4], nor are we in the limit where the number of photons on the detector are high enough to assume a continuous distribution as is done in Goodman (1975) [3]. We therefore employ the discretized P_Γ distribution,$P_{\Gamma\ \mathrm{Discrete}}$ as defined in Chakraborty and Chakravarty (2012) [5]

$$P_{\Gamma\ \mathrm{Discrete}}(k=K|\ \overline{k},\beta)=P_\Gamma(k\le K<k+1\mid\overline{k},\beta)=S(k\mid\overline{k},\beta)-S(k+1\mid\overline{k},\beta) \tag{20}$$

where $S(k|\ \overline{k},\beta)$ is the survival function of the Γ distribution

$$S(k|\ \overline{k},\beta)=\int_k^\infty P_\Gamma(k\mid\overline{k},\beta)\ \mathrm{d}k. \tag{21}$$

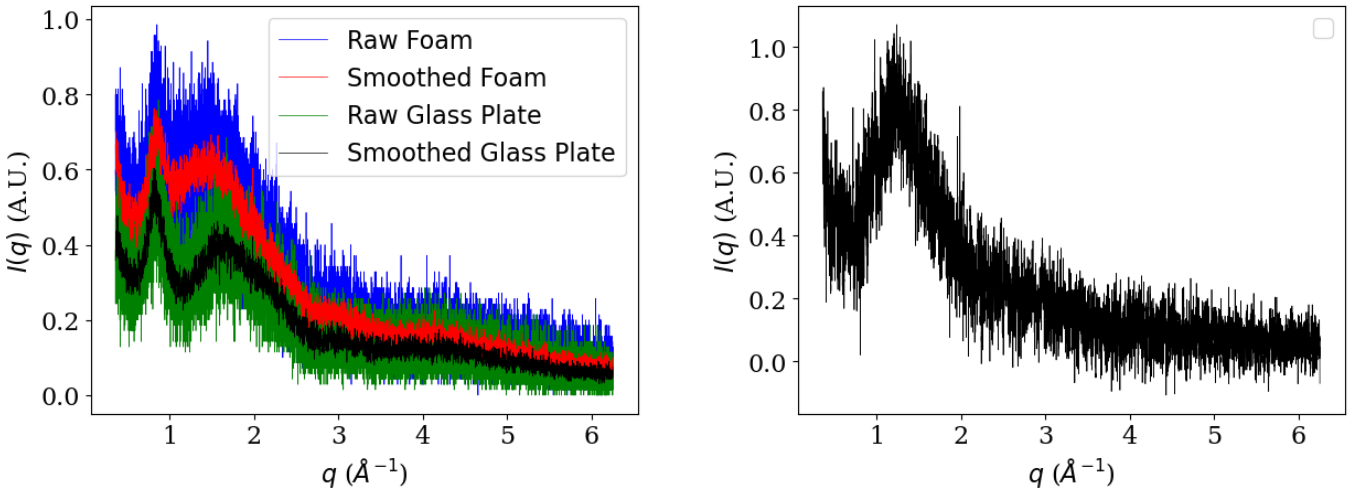

Figure 3: **Left:** Data from in-house X-ray diffraction of the ambient TMPTA foam. To reduce noise on the background subtracted data, we employ a Savitzky-Golay filter (window = 10, polynomial order = 1) to smooth the data. **Right:** $I(q)$ for ambient TMPTA. Data is acquired by subtracting the smoothed foam signal from the smoothed glass and vacuum grease signal. An ambient signal is present at $q = 1.265 \pm 0.317$ Å^{-1}

X-RAY DIFFRACTION CHARACTERISATION OF AMBIENT TMTPA

We present two X-ray diffraction datasets in the paper, one from LCLS and ambient characterization of the foam from Oxford. The latter was taken in Oxford using a Bragg-Brentano geometry.

Powder X-ray diffraction of TMPTA foam

The X-ray wavelength was to $\lambda = 1.54$ Å^{-1}, by applying 40 V to a copper anode. A 0.1 g cm^{-3} TMPTA foam sample, manufactured by Scitech Ltd., was crushed between two glass plates to form a powder. Vacuum grease was used to adhere the powder to the plates during the measurement. Fig. 3 shows the X-ray diffraction signal for the powdered TMPTA and the signal for the glass plate and vacuum grease without the foam. In both the X-ray diffraction data taken in Oxford and the LCLS data, we define the data in the peak position by the half width three quarter maximum of a gaussian fit to the amorphous peak.

Ambient characterization at LCLS

At LCLS, we carried out further analysis of the TMPTA foams. Fig. 4 shows X-ray diffraction of the ambient 0.5 g cm^{-3} foam target and the Kapton wall alone. It is important to note that the X-ray gas monitor failed on the ambient wall characterization shot and so we are unable to use this data to rigorously subtract wall contributions from the ambient and shocked data. We therefore present the scaled data such that signal at high q overlap, absolute intensities should not be compared like for like. Despite the inability to accurately normalize the Kapton wall data, one can observe that there is a greater signal in the foam at low q, perhaps due to the foam's peak at 1.27 Å^{-1}.

In the LCLS setup, we could not resolve the ambient peak at 1.27 Å^{-1} so we only see the tail of this amorphous peak. Without the X-ray gas monitor normalization (and rigorous treatment of self-attenuation), it'd be misleading to claim we can show background subtracted X-ray diffraction for the shocked foam and so we only show qualitative

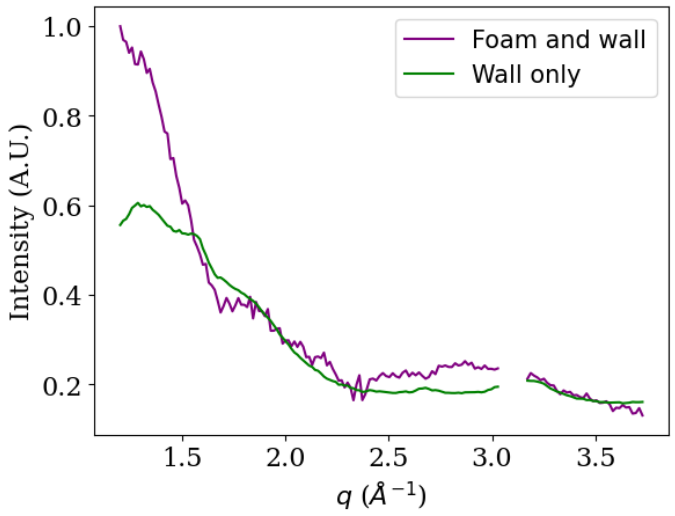

Figure 4: Comparison of wall only and foam and wall ambient X-ray diffraction. Absolute intensity normalization was not possible and so the wall only X-ray diffraction has been scaled to overlap at high q.

movement of the peak in the paper.

[1] D. Zhu, M. Cammarata, J. M. Feldkamp, D. M. Fritz, J. B. Hastings, S. Lee, H. T. Lemke, A. Robert, J. L. Turner, and Y. Feng, A single-shot transmissive spectrometer for hard x-ray free electron lasers, Applied Physics Letters **101** (2012).

[2] J. P. Mithen, J. Daligault, and G. Gregori, Extent of validity of the hydrodynamic description of ions in dense plasmas, Physical Review E—Statistical, Nonlinear, and Soft Matter Physics **83**, 015401 (2011).

[3] J. W. Goodman, Statistical properties of laser speckle patterns, in *Laser speckle and related phenomena* (Springer, 1975) pp. 9–75.

[4] Y. Sun, J. Montana-Lopez, P. Fuoss, M. Sutton, and D. Zhu, Accurate contrast determination for x-ray speckle visibility spectroscopy, Journal of Synchrotron Radiation **27**, 999 (2020).

[5] S. Chakraborty and D. Chakravarty, Discrete gamma distributions: Properties and parameter estimations, Communications in statistics-Theory and Methods **41**, 3301 (2012).